Constraints on the Late Holocene Anthropogenic Contribution to the Atmospheric Methane Budget

Authors: Logan Mitchell[1*], Ed Brook[1], James E. Lee[1], Christo Buizert[1], Todd Sowers[2]

Affiliations:

[1]Oregon State University, College of Earth, Ocean, and Atmospheric Sciences, Corvallis, OR 97331

[2]Department of Geosciences, and Earth and Environmental Systems Institute, Pennsylvania State University, University Park, PA 16802

*Correspondence to: Logan.E.Mitchell@gmail.com

Abstract: The origin of the late pre-industrial Holocene (LPIH) increase in atmospheric methane concentrations has been much debated. Hypotheses invoking changes in solely anthropogenic sources or solely natural sources have been proposed to explain the increase in concentrations. Here two high-resolution, high-precision ice core methane concentration records from Greenland and Antarctica are presented and are used to construct a high-resolution record of the methane inter-polar difference (IPD). The IPD record constrains the latitudinal distribution of emissions and shows that LPIH emissions increased primarily in the tropics with secondary increases in the subtropical northern hemisphere. Anthropogenic and natural sources have different latitudinal characteristics, which are exploited to demonstrate that both anthropogenic and natural sources are needed to explain LPIH methane concentration changes.

One Sentence Summary: A high resolution ice core record of the methane inter-polar difference suggests that both natural and anthropogenic emission increases are needed to explain the methane rise during the late pre-industrial Holocene.

Main Text: The 2.5-fold increase in the concentration of atmospheric methane (CH_4) since the start of the industrial revolution has accounted for ~20% of the total increase in radiative forcing over that time and motivated efforts to understand both natural methane biogeochemistry and anthropogenic impacts on methane sources and sinks (*1*). There has been a lively debate about the impact of early human activities on the global methane budget, stimulated by the observation that atmospheric methane levels generally follow 30°N summer solar insolation over the last 800,000 years, but in the mid-Holocene (~5 thousand years ago, ka) there is a divergence, with methane increasing while insolation decreases. The "early anthropogenic hypothesis" postulates that human activities were responsible for the increase in CH_4 since the mid-Holocene (and CO_2 increases since ~7ka) (*2*) but others argue that the increase originates from natural sources (*3*). Archeological evidence supports early anthropogenic emissions, particularly from rice agriculture (*4, 5*), although the magnitude of those emissions is debated (*3, 6*).

One tool for understanding methane budget changes is the methane Inter-Polar Difference (IPD) (*7-9*) which can be reconstructed from polar ice cores. The IPD is a function of the latitudinal distribution of sources and sinks, as well as the interhemispheric mixing time. The prevalence of northern hemisphere (NH) sources leads to a positive IPD, with higher CH_4 levels recorded in Greenland ice cores than Antarctic ones. Recent work has shown that the main CH_4 sink (OH) is stable on a range of timescales (*10-12*), and we have assumed that there have been no changes in the spatial distribution of OH in the late pre-Industrial Holocene (LPIH). Because interhemispheric transport has a second order effect on the IPD (*13*), source changes are left as the dominant control on IPD variation. Since ~95% of humans lived in the NH tropics and subtropics (0-60°N) during the LPIH (*14*), the fingerprint of anthropogenic emissions would have been an increased IPD relative to the natural background. Indeed, NH anthropogenic

emissions in the industrial age have increased the IPD to ~125 ppb (~7.5% of the mean global concentration), far above the 42 ppb pre-industrial background (~6.4% of the mean global concentration). Here we present decadally resolved ice core methane records from the West Antarctic Ice Sheet (WAIS) Divide and the Greenland Ice Sheet Project 2 (GISP2) ice cores (Fig. 1), which we use to reconstruct the IPD from 800 B.C.E. to 1800 C.E., thus providing data-driven constraints on the early anthropogenic hypothesis.

Our high-precision methane measurements (pooled standard deviation (s.d.) ± 2.4 ppb (*15*)) reproduce multidecadal scale variability observed in a shallow core (WDC05A) (*16*) and in the Law Dome ice core (*15, 17, 18*). We use the WAIS Divide layer counted ice chronology (*19*) and a dynamic firn densification model to construct a gas-age chronology. A Monte Carlo correlation technique using the multidecadal variations is then used to create a GISP2 gas-age chronology synchronized with WAIS Divide (*15*). When comparing the synchronized GISP2 chronology to one constructed independently with a firn densification model and the layer counted ice chronology, we find a difference of 0 ± 11 years, demonstrating that our chronology is robust (*15*). The IPD is calculated by subtracting the WAIS Divide from the GISP2 methane concentration after linear interpolation to annual spacing. Uncertainty bands (1σ) are computed with a Monte Carlo technique incorporating measurement precision and time scale uncertainties (*15*).

The IPD remains essentially constant (781 B.C.E.-1803 C.E. mean 41.6 ppb; trend 0.9 ± 0.3 ppb/ka) throughout the LPIH despite a 115 ppb (17%) increase in the global concentration, broadly consistent with previous low-resolution estimates (Fig. S4) (*8, 17, 20*). The IPD record shows small (~5 ppb) centennial scale variations with a minimum around 250 B.C.E. and maximum around 1100 C.E.

We use an Eight Box Atmospheric Methane Model (EBAMM) after (*21*) to examine hypothesized methane emission scenarios and to compare modeled concentrations with the ice core records (*15*). The model has 6 tropospheric boxes covering 30° latitude each and one stratospheric box per hemisphere. We refer to these boxes as the tropical (0-30°), mid-latitude (30-60°) and high-latitude (60-90°) boxes. The distribution of methane sources is fundamentally under-constrained by concentration data from just the two poles (*22*). However, the modern source distribution provides additional constraints on the relatively small emissions from the 30-90°S and 60-90°N regions (*15*). With these constraints our data can be used in conjunction with EBAMM to solve for the source strength of two latitudinal bands at a time (Fig. S8, (*15*)). We construct three "latitudinal" emission scenarios (L1-3) that balance the global budget and represent the range of realistic emissions. While keeping emissions outside the zonal bands of interest constant, we solve for emissions in the SH vs. NH tropics (L1), tropical (30°S-30°N) vs. mid-latitude NH (L2), and tropical vs. mid to high-latitude NH (L3, Fig. 1). Whenever two EBAMM boxes fall within a latitudinal band we assume a fixed emission ratio between them. L3 is equivalent to a simpler 3-box model (Fig. S9) (*8, 15*). Next we calculate the net change in emissions between 800 B.C.E. and 1400 C.E. in each latitudinal band using linear regression (Table 1). We focus on the time period from 800 B.C.E.-1400 C.E. to avoid the exponential population increase after 1500 C.E and potential natural emission reductions related to the Little Ice Age. Assuming an atmospheric lifetime of 10 years (*12*), scenarios L1-3 show global sources increased ~24 Tg/yr between 800 B.C.E-1400 C.E with the majority of that increase coming from tropical sources (Fig. 1). Varying the methane lifetime from 8-12 years (*12*) caused the increase in global emissions to change by ±5 Tg/yr but did not impact the latitudinal distribution of methane emissions over the LPIH (*15*).

There are two published model-based scenarios of natural wetland methane emission changes during the LPIH (Table 1, Fig. 2). Scenario N1 is based on TRENCH (TRansient Emissions of Natural CH_4), a coarse grid transient model forced by global ice volume, greenhouse gases, and insolation (*23*). Scenario N2 used output from a fine grid methane emissions module tied to a dynamic vegetation model using the climate from the HadCM3 GCM (*3*). These models suggest that global natural methane emissions changed between -2 and 10 Tg/yr between 800 B.C.E and 1400 C.E. for N1 and N2 scenarios, respectively. Neither indicates large decreases in natural methane emissions during the late Holocene in response to declining NH insolation as proposed by the early anthropogenic hypothesis. However, neither model can explain the global increase in methane emissions of ~24 Tg/yr, suggesting that either these models are deficient in some way, or that some amount of anthropogenic emissions are needed to explain the full LPIH CH_4 increase.

Scenarios A1 and A2 utilize two published estimates of anthropogenic emissions for the LPIH while leaving natural emissions constant (to isolate the anthropogenic impact). Scenario A1 uses anthropogenic emission estimates from Houweling et al., (2000) (anthropogenic emissions = 20 Tg/yr at 1500 C.E.) and A2 uses estimates from Ruddiman (2007) (anthropogenic emissions = 43 Tg/yr at 1500 C.E.). To estimate time-dependent anthropogenic emissions we bin global population from the HYDE 3.1 database (*14*) into the EBAMM boxes and define per-capita emissions based on estimates of emissions and population in 1500 C.E. A1-2 assume constant per-capita emissions; scenarios involving changes in per-capita emissions from rice agriculture with time are considered below. The latitudinal distribution of methane emissions from rice agriculture is calculated using population from the rice-producing region of Asia (60-140°E and 10°S-50°N) (*4, 5*). If anthropogenic biomass burning emissions are also

scaled on a per-capita basis the $^{13}CH_4$ isotopic budget increases with time which is inconsistent with the observations (*15, 25*). We therefore keep all biomass burning emissions (natural and anthropogenic) constant; while some small variations are expected based on $\delta^{13}CH_4$ observations (*25*), these lack a long term trend and cannot be systematically tied to population changes on a per-capita basis (*26*). A1 and A2 yield an increase in emissions of 12 Tg/yr and 24 Tg/yr from 800 B.C.E. to 1400 C.E., respectively. As most of the increase in emissions occurred in the NH (Table 1), both scenarios cause the IPD to increase through time which is not observed in the data (Fig. 2). However, increases in global population followed by losses from the Mongol invasion and the spread of the Black Plague in the rice producing portion of Asia (Fig. S12) create a maximum in the modeled IPD from ~1000-1400 C.E. which is observed in the data, lending support to the hypothesis that some of the LPIH increases in emissions were anthropogenic in origin and that variability in population is responsible for some of the variations in the methane record (*16*).

The contribution of natural vs. anthropogenic emissions can be distinguished from their latitudinal distribution (Table 1). Comparing anthropogenic emissions to L1-3, it is clear that scenarios A1-2 both have moderate NH emissions similar to L1-3, whereas N1-2 do not. This suggests that most of the increase in NH emissions is anthropogenic in origin, particularly in the tropical NH (N2 suggests that a small fraction of the mid-latitude NH increase could be natural). In the SH, A1-2 show small increases in emissions since there are minimal population increases in the SH. However, the primary source increase in scenario N2 is SH tropical wetlands, which is consistent with reconstructed increases in the South American monsoon strength (*28*). Since natural wetlands represent the only sizeable source for SH tropical emissions in any of our scenarios, it follows that they are responsible for the majority of the SH emissions identified by

L1-3. Scenario N1 does not show tropical SH increases, possibly because N1 has a lower spatial resolution and simplified climate.

Based on these results we examined scenarios with combined natural and anthropogenic emissions as well as the impact of allowing per-capita emissions from rice agriculture to change through time (*29, 30*). If per-capita emissions from rice agriculture were constant through time, then the best fit to the concentration data is a combination of N2 and A1. However, if we assume the per-capita emissions from rice agriculture decreased linearly by 50% over the LPIH then the larger anthropogenic emissions of A2 combined with N2 provide the best fit (Fig. 2). Larger reductions in per-capita emissions from rice agriculture do not fit the concentration data using our modeling framework (*15*).

Given the current understanding of past population trends and the dependence of methane emissions on climate, our results suggest that increases in both SH natural wetland emissions and a moderate amount of NH anthropogenic emissions are needed to close the LPIH global methane budget. Our concentration dataset provides a constraint for future methane budget modeling efforts focusing on constraining natural and anthropogenic emissions.

References and Notes:

1. P. Forster *et al.*, in *Climate Change 2007: The Physical Science Basis. Contribution of Working Group I to the Fourth Assessment Report of the Intergovernmental Panel on Climate Change,* S. Solomon *et al.*, Eds. (Cambridge University Press, Cambridge, United Kingdom and New York, NY, USA, 2007), pp. 131-234.
2. W. F. Ruddiman, The anthropogenic greenhouse era began thousands of years ago. *Clim. Change* **61**, 261 (Dec, 2003).
3. J. S. Singarayer, P. J. Valdes, P. Friedlingstein, S. Nelson, D. J. Beerling, Late Holocene methane rise caused by orbitally controlled increase in tropical sources. *Nature* **470**, 82 (Feb, 2011).
4. D. Q. Fuller *et al.*, The contribution of rice agriculture and livestock pastoralism to prehistoric methane levels: An archaeological assessment. *Holocene* **21**, 743 (Aug, 2011).
5. W. F. Ruddiman, Z. T. Guo, X. Zhou, H. B. Wu, Y. Y. Yu, Early rice farming and anomalous methane trends. *Quat. Sci. Rev.* **27**, 1291 (Jul, 2008).
6. W. F. Ruddiman, J. E. Kutzbach, S. J. Vavrus, Can natural or anthropogenic explanations of late-Holocene CO2 and CH4 increases be falsified? *Holocene* **21**, 865 (Aug, 2011).
7. I. Fung *et al.*, 3-Dimensional Model Synthesis of the Global Methane Cycle. *J. Geophys. Res.-Atmos.* **96**, 13033 (Jul, 1991).
8. J. Chappellaz *et al.*, Changes in the atmospheric CH_4 gradient between Greenland and Antarctica during the Holocene. *J. Geophys. Res.-Atmos.* **102**, 15987 (Jul, 1997).
9. E. J. Brook, S. Harder, J. Severinghaus, E. J. Steig, C. M. Sucher, On the origin and timing of rapid changes in atmospheric methane during the last glacial period. *Glob. Biogeochem. Cycle* **14**, 559 (Jun, 2000).
10. K. R. Lassey, D. M. Etheridge, D. C. Lowe, A. M. Smith, D. F. Ferretti, Centennial evolution of the atmospheric methane budget: what do the carbon isotopes tell us? *Atmos. Chem. Phys.* **7**, 2119 (2007).
11. S. A. Montzka *et al.*, Small Interannual Variability of Global Atmospheric Hydroxyl. *Science* **331**, (Jan, 2011).
12. V. Naik *et al.*, Preindustrial to present-day changes in tropospheric hydroxyl radical and methane lifetime from the Atmospheric Chemistry and Climate Model Intercomparison Project (ACCMIP). *Atmos. Chem. Phys.* **13**, 5277 (2013).
13. E. J. Dlugokencky *et al.*, Observational constraints on recent increases in the atmospheric CH4 burden. *Geophys. Res. Let.* **36**, (Sep, 2009).
14. K. K. Goldewijk, A. Beusen, P. Janssen, Long-term dynamic modeling of global population and built-up area in a spatially explicit way: HYDE 3.1. *Holocene* **20**, 565 (Jun, 2010).
15. Materials and methods are available as supplementary material on Science Online.
16. L. E. Mitchell, E. J. Brook, T. Sowers, J. R. McConnell, K. Taylor, Multidecadal variability of atmospheric methane, 1000-1800 CE. *J. Geophys. Res.-Biogeosci.* **116**, (Apr, 2011).
17. D. M. Etheridge, L. P. Steele, R. J. Francey, R. L. Langenfelds, Atmospheric methane between 1000 AD and present: Evidence of anthropogenic emissions and climatic variability. *J. Geophys. Res.-Atmos.* **103**, 15979 (Jul, 1998).
18. C. MacFarling Meure *et al.*, Law Dome CO_2, CH_4 and N_2O ice core records extended to 2000 years BP. *Geophys. Res. Let.* **33**, 4 (Jul, 2006).
19. WAIS Divide Project Members, Onset of deglacial warming in West Antarctica driven by local orbital forcing. *Nature* **500**, 440 (08/22/print, 2013).
20. T. Nakazawa *et al.*, Differences of the Atmospheric CH_4 Concentration Between the Arctic and Antarctic Regions in Pre-Industrial/Pre-Agricultural Era. *Geophys. Res. Let.* **20**, 943 (May, 1993).
21. T. Marik, Ph.D., University of Heidelberg (1998).

22. M. A. K. Khalil, R. A. Rasmussen, Sources, Sinks, and Seasonal Cycles of Atmospheric Methane. *Journal of Geophysical Research-Oceans and Atmospheres* **88**, 5131 (1983).
23. T. Y. M. Konijnendijk, S. L. Weber, E. Tuenter, M. van Weele, Methane variations on orbital timescales: a transient modeling experiment. *Clim. Past.* **7**, 635 (2011).
24. S. Houweling, F. Dentener, J. Lelieveld, Simulation of preindustrial atmospheric methane to constrain the global source strength of natural wetlands. *J. Geophys. Res.-Atmos.* **105**, 17243 (Jul, 2000).
25. C. J. Sapart *et al.*, Natural and anthropogenic variations in methane sources during the past two millennia. *Nature* **490**, 85 (2012).
26. O. Pechony, D. T. Shindell, Driving forces of global wildfires over the past millennium and the forthcoming century. *Proc. Natl. Acad. Sci. U. S. A.* **107**, 19167 (Nov, 2010).
27. W. F. Ruddiman, The early anthropogenic hypothesis: Challenges and responses. *Reviews of Geophysics* **45**, 37 (Oct, 2007).
28. X. F. Wang *et al.*, Interhemispheric anti-phasing of rainfall during the last glacial period. *Quat. Sci. Rev.* **25**, 3391 (Dec, 2006).
29. W. F. Ruddiman, E. C. Ellis, Effect of per-capita land use changes on Holocene forest clearance and CO2 emissions. *Quat. Sci. Rev.* **28**, 3011 (Dec, 2009).
30. J. O. Kaplan *et al.*, Holocene carbon emissions as a result of anthropogenic land cover change. *Holocene* **21**, 775 (Aug, 2011).
31. L. E. Mitchell, Oregon State University (2013).

Acknowledgements: This work was supported by NSF OPP grants 0538578, 0520523, 0944584 and 0538538 and by NASA/Oregon Space Grant Consortium grant NNG05GJ85H and the NOAA Climate and Global Change Fellowship Program, administered by the University Corporation for Atmospheric Research (Buizert). We thank two anonymous reviewers who's comments greatly improved the manuscript; Brad Markle, Alex Morin, Brendan Williams, and Jon Edwards for assisting in sample preparation and analysis; Thomas Marik who provided the original 8-box model code (BOSCAGE); Jeff Severinghaus and Giuseppe Etiope who contributed preliminary results from their work; Tiuri Konijnendijk, Jacob Van Etten, and Joy Singarayer who provided model data from their published works; the WAIS Divide Science Coordination Office at DRI, Reno, NV for the collection and distribution of the WAIS Divide ice core (Kendrick Taylor, NSF Grants 0230396, 0440817, 0944348; and 0944266 - University of New Hampshire); NSF OPP which funds the Ice Drilling Program Office and Ice Drilling Design and Operations group for coring activities; NSF which funds the National Ice Core Laboratory which curated and processed the core; Raytheon Polar Services which provided logistics support in Antarctica; and the 109th New York Air National Guard for airlift in Antarctica. Data and description can be downloaded from the NOAA National Climate Data Center http://www.ncdc.noaa.gov/paleo/paleo.html. EBAMM model code is archived with L.E.M.'s Ph.D. thesis (*31*), available online at http://ir.library.oregonstate.edu/xmlui/handle/1957/37906.

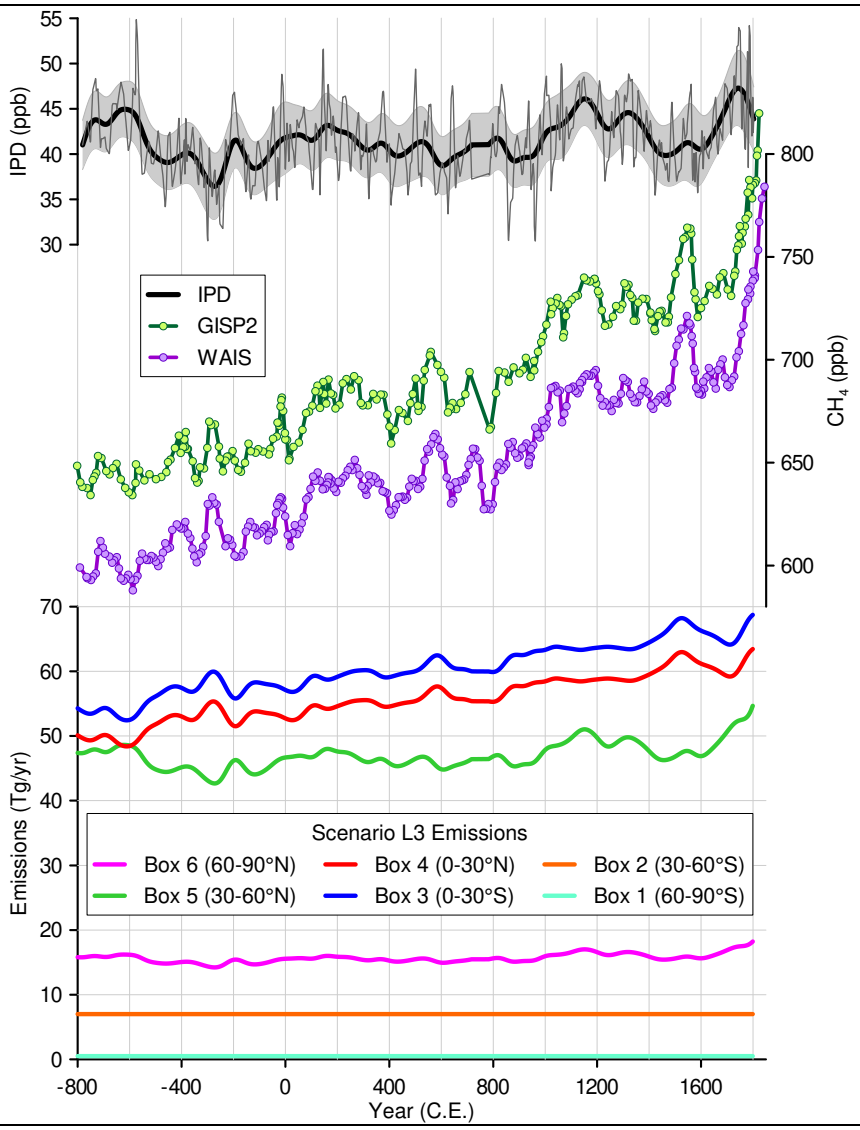

Fig. 1. IPD (top), ice core methane records (middle) and calculated emissions from scenario L3 (bottom). Methane data points show the mean concentration from replicate samples measured at that depth. The thin IPD line shows the IPD obtained by linear interpolation between ice core measurements at an annual spacing and the thick line was computed using a 20-year lowpass filter. The IPD 1σ error bands were obtained using a Monte Carlo procedure accounting for analytical uncertainty of the measurements and chronologic uncertainty of the tie points (*15*).

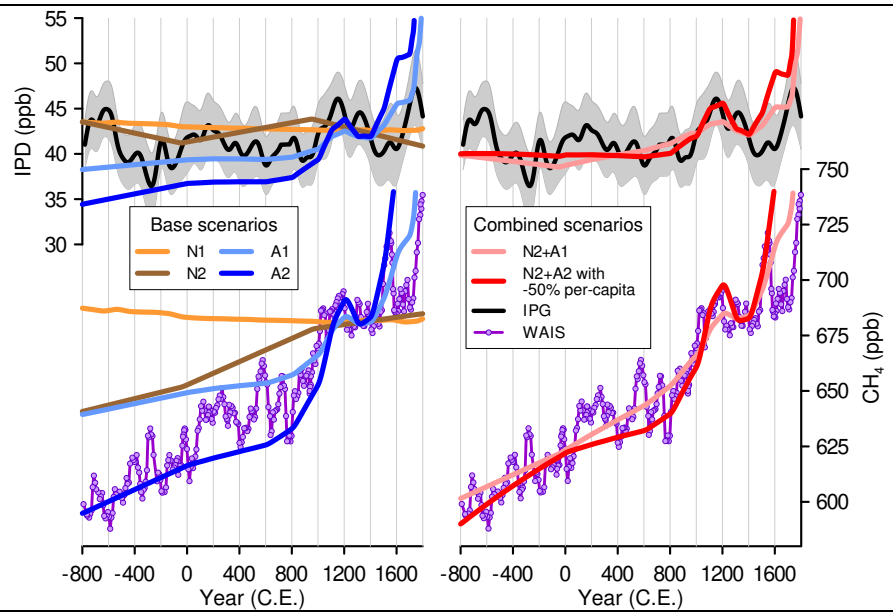

Fig. 2. Modeled methane concentrations from the IPD (top) and Box 1 (60-90°S, bottom) for scenarios N1, N2, A1, and A2 (left) as well as the combined scenarios A1+N2, and A2+N2 with a 50% reduction in per-capita rice agriculture emissions (right). All scenarios are tuned to match the concentration and IPD at ~1400 C.E. Emission histories used to produce these scenarios are shown in Fig. S10. Model concentrations from Box 6 (60-90°N) and Greenland concentration data are omitted for clarity.

Table 1. Modeled change in zonal methane emissions between 800 B.C.E. and 1400 C.E. (Tg/yr), assuming a 10 year methane lifetime. Model scenario labels are: L1-3 solve for total emissions in selected zonal regions. N1-2 have changes in natural emissions only. A1-2 have changes in anthropogenic emissions only. The combined scenarios (N2+A1 and N2+A2 with -50% per-capita) have changes in both natural and anthropogenic emissions.

EBAMM Box (latitude band)	L1*	L2*	L3*	N1	N2	A1	A2	N2+A1	N2+A2 with -50% per-capita
6 (60-90°N)	0	0	1 ± 1	0	-1	0	0	0	0
5 (30-60°N)	0	6 ± 6	3 ± 3	-1	3	4	8	7	6
4 (0-30°N)	18 ± 9	9 ± 3	9 ± 2	-1	1	7	15	7	10
3 (0-30°S)	6 ± 7	9 ± 3	10 ± 2	0	7	1	1	8	8
2 (30-60°S)	0	0	0	0	0	0	0	0	0
1 (60-90°S)	0	0	0	0	0	0	0	0	0
Total change	24 ± 4	24 ± 4	23 ± 4	(-2)	10	12	24	22	24
CH_4 increase (ppb)	93	92	92	(-6)	41	43	92	84	94

* The difference in the zonal methane emissions between 800 B.C.E. and 1400 C.E. (± 2 times the 1 σ standard deviation of the prediction interval) after calculating the linear regression of emissions from the global methane budget solved for tropical and subtropical NH emissions. In L1-3 we solve for the zonal bands indicated by the colors; when there are two boxes within a band we assume a fixed emission ratio between them. See the supplementary materials for details.